
Relay Variational Inference: A Method for Accelerated Encoderless VI

Amir Zadeh, Santiago Benoit, Louis-Philippe Morency
Language Technologies Institute, Department of Computer Science
Carnegie Mellon University
Pittsburgh, PA 15213
{abagherz,sbennoit,morency}@cs.cmu.edu

Abstract

Variational Inference (VI) offers a method for approximating intractable likelihoods. In neural VI, inference of approximate posteriors is commonly done using an encoder. Alternatively, encoderless VI offers a framework for learning generative models from data without encountering suboptimalities caused by amortization via an encoder (e.g. in presence of missing or uncertain data). However, in absence of an encoder, such methods often suffer in convergence due to the slow nature of gradient steps required to learn the approximate posterior parameters. In this paper, we introduce Relay VI (RVI), a framework that dramatically improves both the convergence and performance of encoderless VI. In our experiments over multiple datasets, we study the effectiveness of RVI in terms of convergence speed, loss, representation power and missing data imputation. We find RVI to be a unique tool, often superior in both performance and convergence speed to previously proposed encoderless as well as amortized VI models (e.g. VAE).

1 Introduction

Variational Inference (VI) offers a method for sampling from intractable posteriors in machine learning [8]. It relies on using approximate posteriors: essentially well-known distributions that make the process of sampling from the latent space possible. Commonly in VI, inference is done using parametric models [3], such as a probabilistic encoder in VAE [11]. Using a parametric model to perform inference allows for fast inference given new datapoints. However, encoders can also produce suboptimal approximations of the posteriors [2], especially when inference is done over uncertain inputs, e.g. with missing data [14]. Such suboptimalities in the encoder can in turn lead to suboptimal optimization of the variational objective (Evidence Lower Bound - ELBo).

Inference of the approximate posterior parameters can be done optimally without relying on an encoder; using stochastic gradient-based optimization of the approximate posterior parameters directly [14]. Encoderless models offer an intriguing perspective of VI, one that is robust to presence of noise or missing data, as well noise distribution disparity between train and test stages. However, their main shortcoming is their reliance on slow incremental optimization in inference of approximate posterior parameters. This slow nature is further intensified by the fact that approximate posterior parameters for the datapoints are optimized independently, due to the mean-field assumption as part of encoderless VI¹.

In this paper, we introduce Relay Variational Inference (RVI). RVI is a general (blackbox) neural VI framework that utilizes “relays” within the latent space to speed up the optimization of the variational

¹as opposed to encoder-based inference where updates incrementally make the encoder better at posterior approximation for all the datapoints.

objective. The relays essentially exploit the commonalities between datapoints according to their formulation (Section 3). Subsequently, the gradient of the objective can flow between datapoints, essentially mitigating the slow nature of mean-field approximation. This in turn decreases the number of gradient steps during training and inference, thus increasing the overall speed. We summarize the characteristics of the proposed method as follows:

- RVI maintains the appealing properties of encoderless VI, including optimal inference as well as robustness to noisy or missing data, while speeding up the training and inference process.
- The benefits of RVI come without requiring extra sampling steps, loss terms, or arduous increase in number of learnable parameters.
- It is also simple to implement, and flexible in the manner in which the relay can be calculated and interpreted.

2 Related Works

In deep learning, inference of approximate posteriors in VI is commonly done with encoders (i.e. inference networks). While amortizing the posterior inference has benefits when it comes reducing the time required for this crucial step of VI, it can also suffer from suboptimalities [2], especially in presence of uncertain input (e.g. missing data) [14]. Previous works have attempted to mitigate the inference suboptimality of encoders using fine-tuning [5], ladder-based models [13], or Hessian-based finetuning after initial training [9]. While designed for particular architectures (e.g. RNNs), or limited by the maximum number of learnable parameters (due to Hessian calculations), generalizable extensions of such models require further research.

More relevant to this paper, are the works that rely on updating the approximate posteriors using a gradient-based optimization pipeline [7, 14]. Such models directly optimize the parameters of the posterior distribution, which can mitigate the suboptimalities of an amortized framework. They can also remain robust in presence on noise or missing data. However, the updates of such gradient-based posterior approximation frameworks can be slow and unsteady [4]. They remain susceptible to the choice of training parameters such as learning rate. A common cause of the slow and unsteady nature of their training is the full independence (mean-field assumption) imposed by the gradient-based posterior approximation methods [6]. Making strong assumptions about the hierarchy in the latent space and enforcing extra loss terms on the VI is proposed to mitigate this issue [12]. However, such strong assumptions may introduce unnecessary variances on both the latent space and the learning framework.

Through usage of relay, the method in this paper proposes a way to break the mean-field assumption, without requiring strong assumptions on the latent space (e.g. through new loss terms in the VI objective). Furthermore, the relays can take many flexible configurations to offer interpretable concepts such as hierarchies and clusters.

3 Model

Let $\mathcal{D} = \{x_i \sim p(x); x \in \mathbb{R}^d\}_{i=1}^N$ be a given datasets. d denotes the dimensionality of individual datapoints. Given this dataset, the goal is to learn a parametric distribution $p_\theta(x)$, with learnable parameters θ . The generative process of the dataset is considered as $p(z)p(x|z)$, where a sample of the latent space $z_i \sim p(z)$ is used to create the datapoint x_i using the conditional distribution $p(x|z)$. However, this would require calculation of the true posterior $p(z|x)$ during train time, which is often hard to calculate for nonlinear decoders without MCMC.

Instead of true posterior, an approximate posterior q can be marginalized over during training, with the condition that $q(z|x_i, \phi) > 0$ if $p(z|x_i, \theta) > 0$. Using this approximate posterior, the likelihood of the model parameters given the data can be written as:

$$\mathcal{L}(\theta|x_i) = \text{KL}\left(q_\phi(z|x_i) \parallel p_\theta(z|x_i)\right) + \mathcal{V}(q_\phi, \theta|x_i) \quad (1)$$

$\mathcal{V}(\cdot)$, often referred to as ELBo, can be written as:

$$\mathcal{V}(q_\phi, \theta|x_i) = \mathbb{E}_{q_\phi(z|x_i)} \left[\log p_\theta(x|z) \right] - \text{KL} \left(q_\phi(z) \parallel p_\theta(z) \right) \quad (2)$$

In presence of missing data, the first term of the RHS in Equation 2 marginalizes over the missing dimensions [14].

In Relay Variational Inference framework, the parameters of the local approximate posterior distributions can be written as:

$$\phi_i = \phi_i^R + \phi_i^\epsilon \quad (3)$$

In the above formulation, ϕ_i^R is called the relay. It is a factor that binds a set of datapoints together thus breaking the mean-field assumption of the stochastic optimization process. It’s main role is to and allow for propagation of the gradient among the datapoints. The formulation of the relay can take different forms, and is discussed in the next section. ϕ_i^ϵ is a stochastic variable that is unique to individual datapoints.

3.1 Formulation of ϕ_i^R

The relay ϕ_i^R is essentially a shared factor among the datapoints. The calculation of ϕ_i^R can take different forms², but in this section we discuss one particular approach that offers fast convergence without sacrificing the learning performance. Let $R = \{r_k \in \mathbb{R}^t\}_{k=1}^K$ be a set of K independent stochastic vectors within the latent space with t dimensions. These K vectors can in turn be used to approximate the position of a given data point within the latent space. This is formulated as follows:

$$\phi_i^R = \sum^{b_i \in K} a_{b_i} \cdot r_{b_i} \quad (4)$$

Where $B_i = \{b_i \in K\}$ are indicators for the different vectors in R , and a_{b_i} are coefficients for vectors r_{b_i} . In simple terms, i th datapoint is assigned to a subset of vectors $\{b_i \in K\}$ with coefficients a_{b_i} . The relay is a direct linear combination of the subset as shown in Equation 4, which in turn defines the position of the approximate posterior parameters in the latent space, according to the Equation 3.

In reality, without complicating the notation³, there can be multiple sets of vectors R , defining multiple groups of vectors which a datapoint is defined based on. For example, a first small set can be defined with only a few vectors to capture the holistic variations among datapoints, while a subsequent group with larger number of vectors can capture the differences across the datapoints. The ϕ_i^R is calculated for each of the different groups according to Equation 4. The calculated relays based on each group can subsequently be summed to calculate the position of a final relay which will be used in Equation 3. In most of our experiments, we use the combination of three groups with 25, 50 and 100 vectors. Each datapoint is assigned to only a total of $|B_i|$ vectors in each group ($|B_i|$ can change from one group to another). In each group, the choice of which vectors will be assigned to the datapoint is done by first calculating the coefficients for all vectors, and subsequently choosing them based on the top $|B_i|$ coefficients according to their absolute value (e.g. top 10 absolute values in a group of 50 vectors).

4 Learning

Learning can be done by maximizing the lower bound in Equation 2. Using Equations 3 and 4, Equation 2 is differentiable w.r.t R (or multiple R s if there exist multiple groups), a_{b_i} and ϕ_i^ϵ . All these learnable variables together define the parameters of the approximate posterior for each data point. They can be initialized randomly, and optimized as stochastic variables using gradient-based methods, alongside the parameters θ of the decoder. After training is done, for new datapoints, Equation 2 is used to optimize a_{b_i} (assignment coefficients) and ϕ_i^ϵ . R and θ are the parameters of the model, and remain fixed during testing.

²A comprehensive set of such forms with their characteristics are discussed in supplementary, including mixture models and clusters.

³Full notation and calculation provided in supplementary.

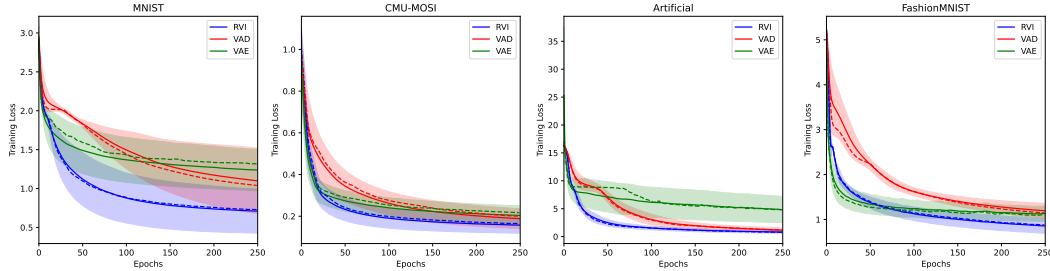


Figure 1: Convergence analysis of the compared models in this paper, across a range of hyperparameters discussed in Section 6.1. Dotted line displays the median performance. Overall, RVI (blue) maintains superior average loss than both VAE (green) and VAD (red).

Since RVI introduces no new distribution or loss term to the lower bound in Equation 2, sampling during generation remains the same as conventionally done in literature [11].

While learning is done using the ELBo objective, to have a universally understandable sense of model performance in our experiments, we report the elastic metric (L1+L2, lower better) for the reconstruction done based on drawing the mean of the approximate posterior distributions.

5 Methodology

In this section, we outline the methodology for the experiments of this paper. We first discuss the datasets and baselines, followed by a discussion of the network architecture used in our experiments.

5.1 Datasets and Baselines

MNIST and Fashion-MNIST: MNIST and Fashion-MNIST⁴ are datasets of 28×28 grayscale images which contain 10 classes of digits or fashion items. We use the standard folds of the two datasets.

CMU-MOSI Dataset: CMU Multimodal Sentiment Intensity (CMU-MOSI) is an in-the-wild dataset of multimodal sentiment analysis [15]. The dataset contains 2199 opinionated sentence utterances, with three modalities of text (words), vision (gestures) and acoustic (sound). The labels are sentiment scores between $[-3, 3]$. Feature extraction on this dataset is similar to [1]. We use the standard released folds⁵.

Toy Artificial Dataset: We use a similar artificial dataset as used by [14]. The input space of this dataset is 300 dimensions. It is generated based on linear combination of samples drawn from 10 different distributions such as Normal, Beta and Gumbel.

The following main baselines are used for comparison in our experiments. Further baselines in Section 2 are studied in the supplementary.

VAE: Variational AutoEncoder (VAE) [11] is an amortized neural VI model. It relies on an encoder to approximate the posterior distribution conditioned on a given datapoint. During training, the parameters of the encoder are learned alongside the decoder in an end-to-end fashion.

VAD: Variational AutoDecoder (VAD) [14] is a VI method specifically useful for learning from missing data. Unlike a VAE which relies on an encoder to approximate the posterior of the data, VAD does so using an iterative optimization process over the ELBo loss (with the missing dimensions marginalized).

5.2 Neural Decoder Architecture

In this paper, we perform our experiments using three different neural architectures. The main decoder architecture uses two hidden layers of [64, 64] neurons between the latent space (64 neurons) and the

⁴<https://github.com/zalandoresearch/fashion-mnist>

⁵<https://github.com/A2Zadeh/CMU-MultimodalSDK>

output space (same dimension as the input space). Hidden layers are activated using ReLU, with the final layer having linear activation. For VAE, the encoder is the reverse architecture of the decoder. Two auxiliary architectures are also studied in Section 6 and more in depth in the supplementary⁶. These architectures are one-layer decoder with [64] hidden units, and three-layer decoder [64, 64, 64] hidden units. Similarly, they use ReLU as hidden layer activation and linear as final layer. Overall, in our experiments we observe closely similar baseline performance trends for the auxiliary architectures and the main architecture.

6 Experiments

In this section, we outline a comprehensive set of experiments to understand the performance of RVI in detail. We recommend viewing the figures in color, and zoomed in if necessary. We recommend viewing the figures in color, and zoomed in if necessary. We put the primary focus on the first term of the variational inference for our experiments. The first term is what experiences instability due to missing values, with the second term being identical across different variational baselines in this paper.

6.1 Training Convergence

We compare the convergence rate of the RVI, VAE, and VAD during training. This convergence analysis is performed over an extensive hyperparameter search space. The hyperparameters include the learning rates of $\{0.01, 0.001, 0.0001, 0.00001\}$ (for both the network θ and approximate posterior parameters ϕ_i^R and ϕ_i^ϵ), 3 different decoder architectures [64], [64, 64], [64, 64, 64] (encoder is the inverse of the decoder for VAE), and Missing Completely at Random (MCAR) missing rates of $\{0.1, 0.2, 0.3, 0.4, 0.5, 0.6, 0.7, 0.8, 0.9\}$. Each hyperparameter set is trained 10 times. Figure 1 shows the mean, standard deviation and median of the elastic metric for all the hyperparameter runs. It highlights the average behavior of the models over the entire set of trained hyperparameters. The results of this experiment demonstrate that RVI is able to perform superior and converge fast than both VAE and VAD.

Aside a holistic view of performance across different hyperparameters, we also study how the models perform using the commonly used learning rate of 0.001 for Adam [10] (across all parameters θ , ϕ_i^R and ϕ_i^ϵ). The decoder is the main 2 layer network discussed in Section 5.2. Figure 2 compares the 3 models side by side. The rows demonstrate the MCAR missing rates of 0.0 (no missing data), 0.5, and 0.9. The columns are the datasets used in the experiment. Overall, RVI shows superior performance than VAE and VAD.

6.2 Test Performance

We compare the models in this paper for the generalization of their performance over the test set. The testing is performed after the models are trained for a full 250 epochs. The missing rate studied in this case are MCAR with rates of $\{0.1, 0.2, 0.3, 0.4, 0.5, 0.6, 0.7, 0.8, 0.9\}$. Figure 3 shows the test loss for the compared models over different missing rates. Standard deviations are calculated over 10 runs of each hyperparameter set. We also extend this experiment to the task of missing data imputation. After inference is done using RVI, VAD or VAE, we reveal the missing components of each datapoint to calculate the imputation loss. Figure 4 shows the imputation performance of the compared models.

Further studies of the latent space (including interpolations and visualizations), as well as results for other missing patterns are covered in supplementary.

6.3 Supervised Analysis

While comparing the learned approximate posteriors in terms of how well their reconstructions resemble the datapoints is important, we also study the strength of the learned representations when used for supervised tasks. We first learn the representations from a dataset using the variational objective in Equation 2, and subsequently use the representations (ϕ_i) as input to a supervised model. For learning representations, we use the main network in Section 5.2. We use the MNIST and the more challenging Fashion-MNIST variant, with their standard folds. We change the missing rate from

⁶We also study the effect of latent space shape in the supplementary.

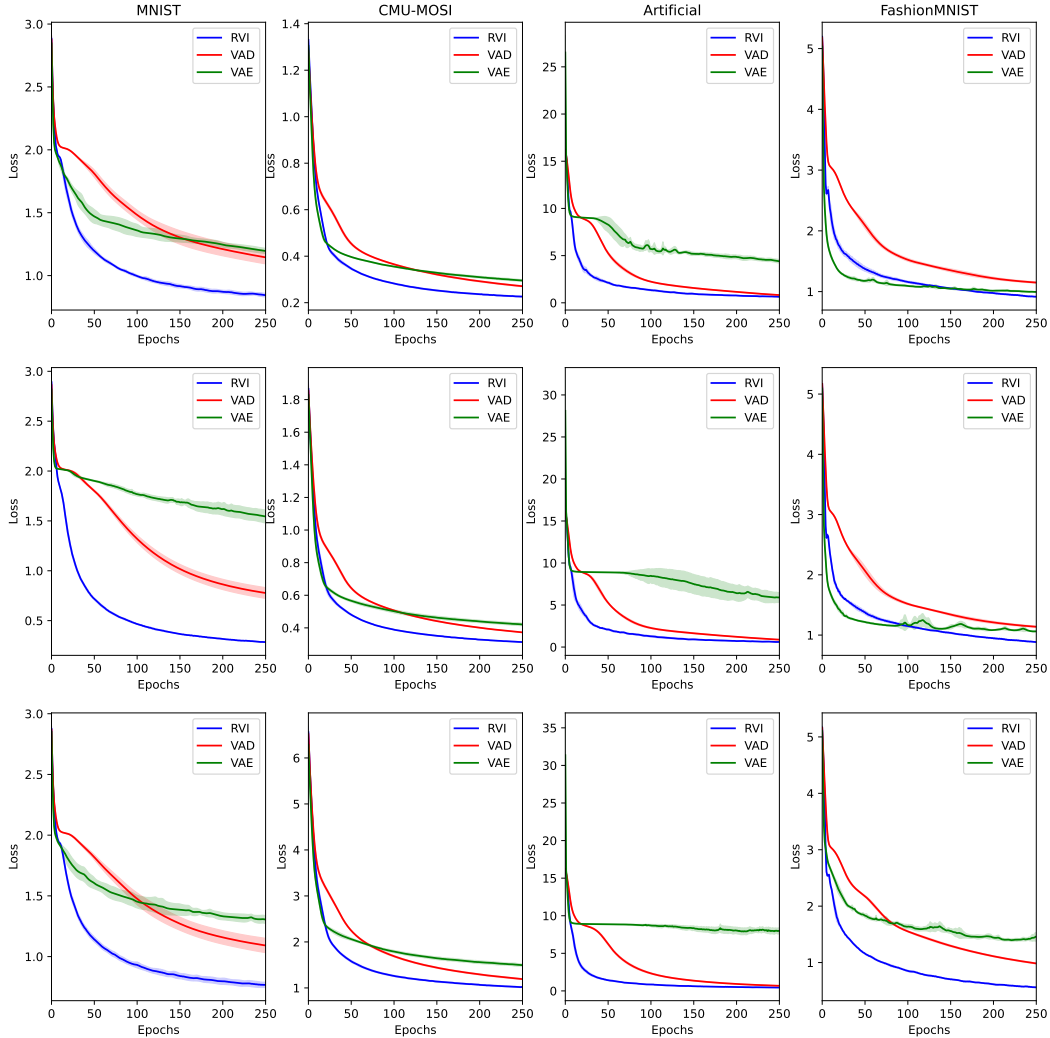


Figure 2: Convergence comparison between the proposed RVI (blue) framework, VAD (red), and VAE (green) applied on the main network discuss in Section 6. Training is performed using the commonly used learning rate of 0.001 for Adam. First, second and third row are for 0.0, 0.5, and 0.9 missing rates respectively. Generally, RVI converges faster, and to a better loss than baselines.

0.0 to 0.9 in increments of 0.1. Representations are trained for 250 epochs, and subsequently used to train a supervised model with 64 hidden neurons (ReLU activated) for 250 epochs. Training is done 10 times to calculate standard deviations. Learning rate for all networks and approximate posteriors is 0.001. Figure 5 shows the results of this experiment. The first row shows the classification loss (categorical cross-entropy) when training the classification network, and the second row shows the accuracy over test set. Overall, the representations learned by RVI offer faster convergence and more accurate predictions across different learning rates.

6.4 Posterior Approximation Learning Rate

While in the previous experiments, the learning rate of the network and the approximate posteriors are the same, in reality, the approximate posterior can have a different learning rate than the network. This change in learning rate can possibly affect the convergence, and needs to be studied for both RVI and VAD (VAE has no such hyperparameter therefore excluded from this experiment). We use the main network in Section 5.2, with the learning rate of 0.001 for θ . The approximate posterior learning rates is chosen from $\{0.01, 0.005, 0.001, 0.0005, 0.0001, 0.00005, 0.00001\}$. The dataset is

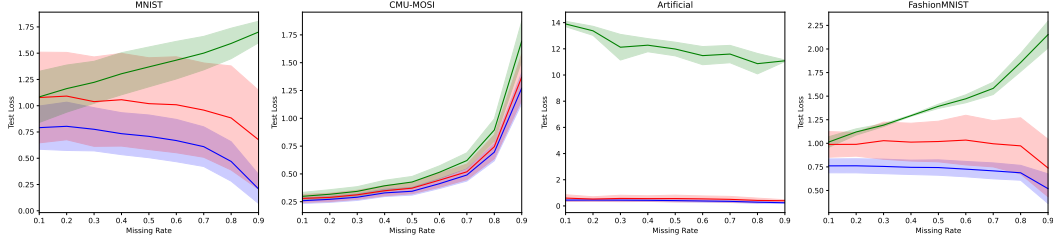


Figure 3: Comparison of RVI (blue), VAE (green) and VAD (red) over different MCAR missing rates at test time. The loss is calculated over the available (non-missing) portions that are used for the inference. RVI outperforms both VAE and VAD in generalization to test set.

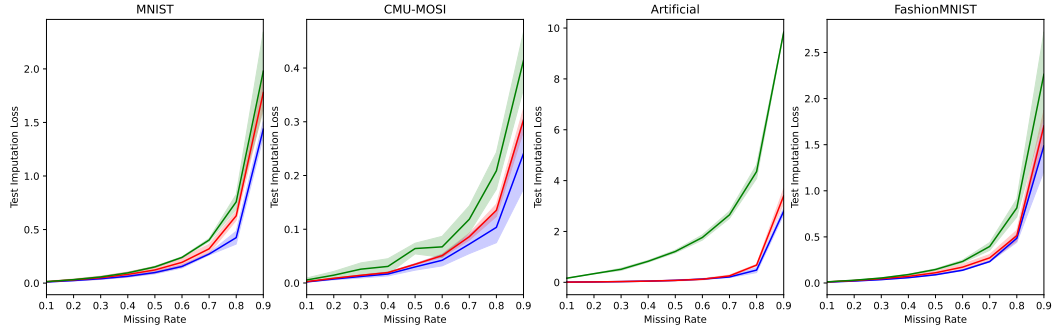


Figure 4: Comparison of RVI (blue), VAE (green) and VAD (red) for missing data imputation at test time over different MCAR missing rates. After inference, the missing data is revealed to calculate the loss (thus missing components are never used during inference). This shows that while RVI is faster than VAD, it can also achieve similar or superior performance in imputation.

MNIST with no missing data. We study the convergence rate for both train and test sets in Figure 6. We observe that during both training and testing, RVI achieves better loss than the VAD. The results also signal that for the best convergence, it is better to use high learning rate during training of RVI but use a lower one during validation.

6.5 Relay Structure

We study the effect of the relay structure, as well as the effect of the different groupings discussed in Section 3.1. The models are trained on MNIST dataset. The network used is the main network discussed in Section 5.2. Learning rate of 0.001 is used for both the network and the approximate posteriors. There are three groups of relays as defined in Section 3.1 which include $\{25, 50, 100\}$ vectors each. Figure 7 shows the progressive contribution of each of the groups to the final reconstruction of the input images (at MCAR rate of 0.5). The results show that the relays in each group contribute to the final reconstruction of the datapoints. Furthermore, the group with 25 vectors captures the general appearance of the digit with 50 and 100 capturing further variations needed for reconstructing the datapoints.

7 Conclusion

In this paper, we presented the Relay Variational Inference (RVI) framework. Using relays, RVI is able to bind datapoints together and mitigate the mean-field assumption required for encoderless VI. The relay is designed to improve the performance and convergence rate of encoderless VI. We perform experiments over multiple datasets, and compare the RVI to VAE and VAD. RVI reaches better loss, and in most cases converges faster than both VAE and VAD. It’s performance generalizes to missing data imputation, performing similar or better than VAD. Furthermore, the representations learned by RVI are studied for supervised learning, and show to be superior to VAE and VAD.

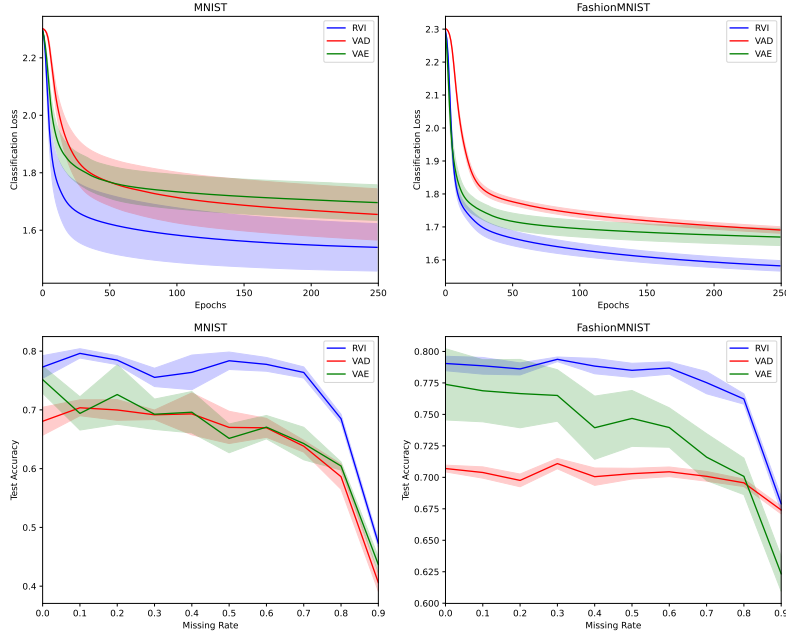


Figure 5: Comparison of convergence speed and accuracy of trained models over representations learned by RVI (blue), VAE (green) and VAD (red). The representations learned by RVI offer faster downstream supervised convergence and more accurate predictions.

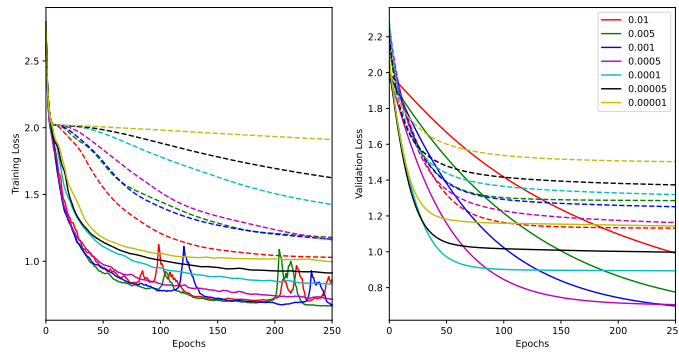


Figure 6: The effect of the approximate posterior learning rate over training speed for RVI (solid) and VAD (dotted). MNIST dataset is used, and network learning rate is 0.001. Learning rate search space includes 7 different learning rates color coded in the figure.

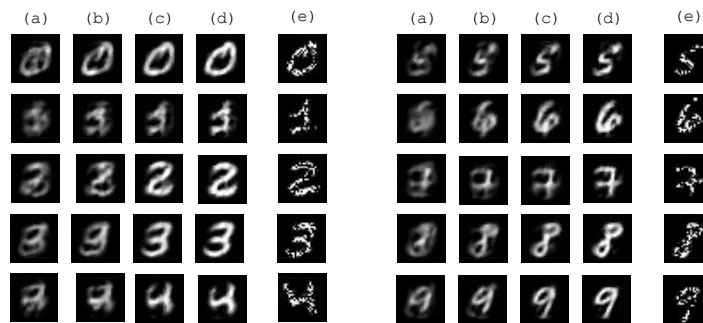


Figure 7: Reconstruction progression of the proposed RVI framework. (e) is the input to the RVI model, and (d) is the final reconstruction. (a) is the reconstruction using only the first group of 25 relays, (b) is the contribution of the two groups of $\{25, 50\}$ and (c) is the contribution of all groups $\{25, 50, 100\}$. (d) includes the contribution from ϕ_i^ϵ .

References

- [1] Minghai Chen, Sen Wang, Paul Pu Liang, Tadas Baltrušaitis, Amir Zadeh, and Louis-Philippe Morency. Multimodal sentiment analysis with word-level fusion and reinforcement learning. In *Proceedings of the 19th ACM International Conference on Multimodal Interaction*, pages 163–171. ACM, 2017.
- [2] Chris Cremer, Xuechen Li, and David Duvenaud. Inference suboptimality in variational autoencoders. *arXiv preprint arXiv:1801.03558*, 2018.
- [3] Peter Dayan, Geoffrey E Hinton, Radford M Neal, and Richard S Zemel. The helmholtz machine. *Neural computation*, 7(5):889–904, 1995.
- [4] Akash Kumar Dhaka, Alejandro Catalina, Michael Riis Andersen, Måns Magnusson, Jonathan H Huggins, and Aki Vehtari. Robust, accurate stochastic optimization for variational inference. *arXiv preprint arXiv:2009.00666*, 2020.
- [5] Devon Hjelm, Ruslan R Salakhutdinov, Kyunghyun Cho, Nebojsa Jojic, Vince Calhoun, and Junyoung Chung. Iterative refinement of the approximate posterior for directed belief networks. In *Advances in Neural Information Processing Systems*, pages 4691–4699, 2016.
- [6] Matthew D Hoffman and David M Blei. Structured stochastic variational inference. In *Artificial Intelligence and Statistics*, pages 361–369, 2015.
- [7] Matthew D Hoffman, David M Blei, Chong Wang, and John Paisley. Stochastic variational inference. *The Journal of Machine Learning Research*, 14(1):1303–1347, 2013.
- [8] Michael I Jordan, Zoubin Ghahramani, Tommi S Jaakkola, and Lawrence K Saul. An introduction to variational methods for graphical models. *Machine learning*, 37(2):183–233, 1999.
- [9] Yoon Kim, Sam Wiseman, Andrew C Miller, David Sontag, and Alexander M Rush. Semi-amortized variational autoencoders. *arXiv preprint arXiv:1802.02550*, 2018.
- [10] Diederik P Kingma and Jimmy Ba. Adam: A method for stochastic optimization. *arXiv preprint arXiv:1412.6980*, 2014.
- [11] Diederik P Kingma and Max Welling. Auto-encoding variational bayes. *arXiv preprint arXiv:1312.6114*, 2013.
- [12] Rajesh Ranganath, Dustin Tran, and David Blei. Hierarchical variational models. In *International Conference on Machine Learning*, pages 324–333. PMLR, 2016.
- [13] Casper Kaae Sønderby, Tapani Raiko, Lars Maaløe, Søren Kaae Sønderby, and Ole Winther. Ladder variational autoencoders. In *Advances in neural information processing systems*, pages 3738–3746, 2016.
- [14] Amir Zadeh, Yao-Chong Lim, Paul Pu Liang, and Louis-Philippe Morency. Variational auto-decoder: Neural generative modeling from partial data. *arXiv preprint arXiv:1903.00840*, 2019.
- [15] AmirAli Bagher Zadeh, Paul Pu Liang, Soujanya Poria, Erik Cambria, and Louis-Philippe Morency. Multimodal language analysis in the wild: Cmu-mosei dataset and interpretable dynamic fusion graph. In *Proceedings of the 56th Annual Meeting of the Association for Computational Linguistics (Volume 1: Long Papers)*, volume 1, pages 2236–2246, 2018.

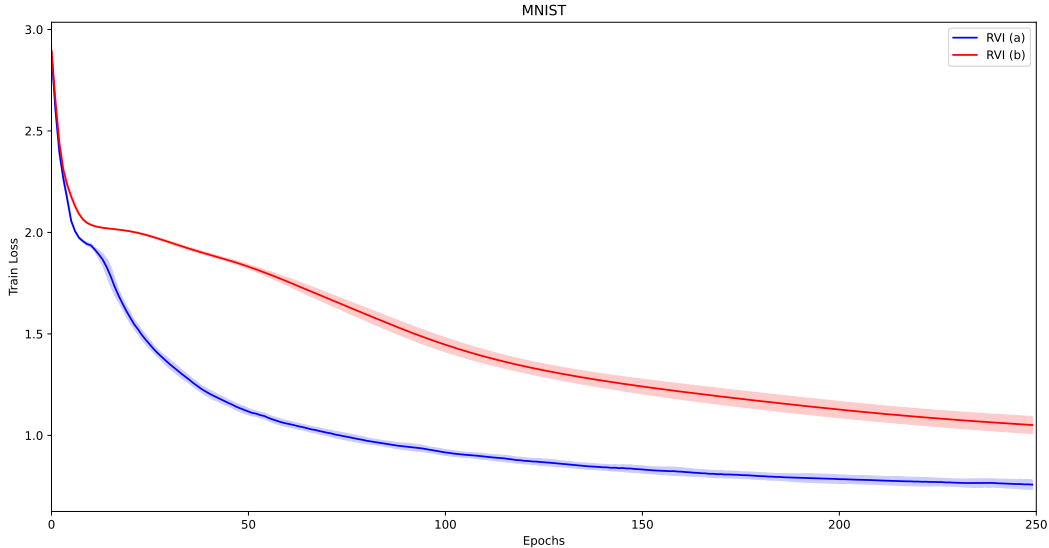


Figure 8: Results for the experiments in Section A. RVI (a) is with the clustering relay formulation and RVI (b) is the method used in the body of the paper. The latter shows faster convergence to a better loss.

Appendices

A Relay Formulations

The formulation of relay ϕ_i^R can take many different forms. However, in this paper we study two cases. The first is discussed in the main body of the paper. The second case is the case of assigning the datapoints to only a single vector in each relay group (essentially $|B_i| = 1$, for each relay group). This essentially forms clusters of datapoints in the latent space, where each datapoint is assigned to one relay. For this, similar to the experiments in the main body of the paper, we utilize 3 groups of $\{25, 50, 100\}$, and compare it with the main formulation in the paper.

B Effect of $|B_i|$ on the Convergence of RVI

$B_i = \{b_i \in K\}$ essentially controls how many shared vectors in the latent space each datapoint connects to, for the formulation in the main body of the paper. In our experiments, we change the proportion of $\frac{|B_i|}{K} \in \{0.1, 0.2, 0.3, 0.4, 0.5, 0.6, 0.7, 0.8, 0.9\}$. This essentially means each datapoint can connect (via coefficients a_i). We use the groupings of $\{25, 50, 100\}$ vectors. For example, for the case of 0.8, that would mean each datapoint can connect to $\{20, 40, 80\}$ from the original set of vectors. Results in Figure 10 show the convergence for this experiment. MNIST with 0.5 MCAR missing rate is used with learning rate of 0.001 for all the learnable parameters of RVI. $\frac{|B_i|}{K}$ offers a tradeoff between performance in loss and performance in computational cost. However, we observe that 0.5 is a suitable for outperforming VAE and VAD in most cases.

In order to compare the effect of having different groupings at training time, we use three sets of groupings to train the RVI model: $\{25\}$, $\{25, 50\}$ and c. Table 9 visually shows the training results. We observe that having different groups is beneficial for the final quality of reconstructions.

C Parameterization of the ϕ_i and Calculation of ELBo

In order to calculate the variational lower bound in Equation 2, the approximate posteriors can be defined as a multivariate normal distribution:

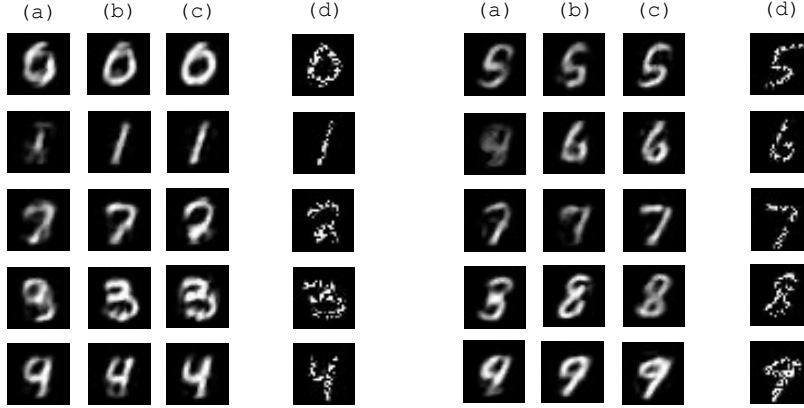


Figure 9: Effect of relay configuration on the final reconstructions. Column (a) uses a single group of [25] vectors, (b) uses double layers of [25, 50] and columns (c) uses groups of [25, 50, 100]

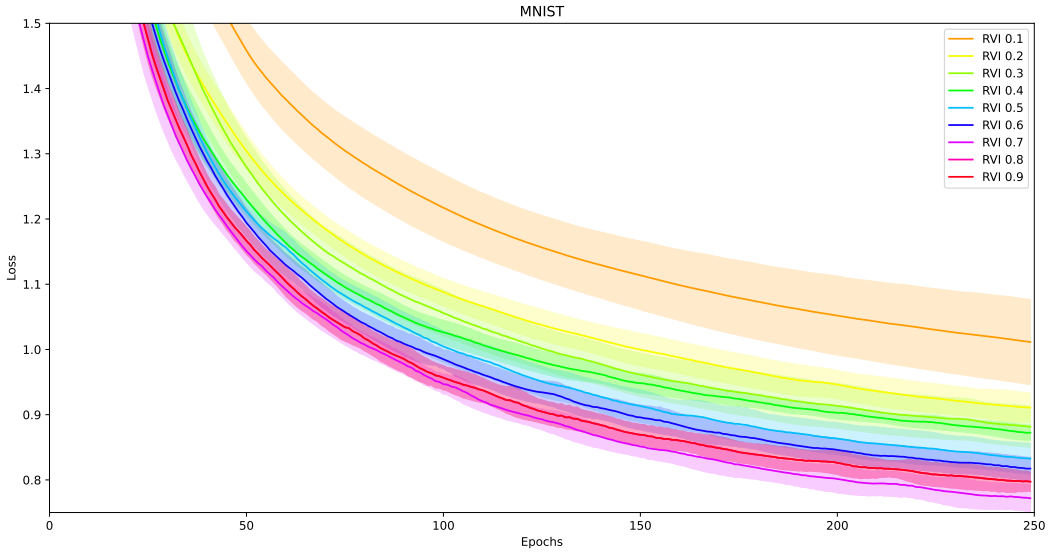


Figure 10: Convergence comparison for different ratios of $\frac{|B_i|}{K} \in \{0.1, 0.2, 0.3, 0.4, 0.5, 0.6, 0.7, 0.8, 0.9\}$ as discussed in Appendix B. Results are zoomed in to better show the distinction.

$$q_\phi(z|x_i) = \mathcal{N}(z; \mu_i^R + \mu_i^\epsilon, \Sigma_i) \quad (5)$$

With the μ_i^R as the mean calculate via the relay formulation, and μ_i^ϵ the individual deviations from the relay. Σ_i is the standard deviation. Samples $z \sim q_\phi(\cdot)$ can then be defined as $z = \mu_i^R + \mu_i^\epsilon + \lambda \cdot \Sigma_i$, and $\lambda \sim \mathcal{N}(0, I)$. Subsequently, Equation 2 becomes differentiable to the samples drawn based on the Equation 5, essentially being differentiable w.r.t both ϕ_i^R and ϕ_i^ϵ . The final calculation depends on the choice for $p_\theta(x|z)$ - which in this paper is similar to [14]. The missing data will not partake in the calculation of the loss via marginalization.

Similarly, after training is done, samples can be drawn using the same reparameterization trick, or alternatively sampling using the second term in the RHS of Equation 2.

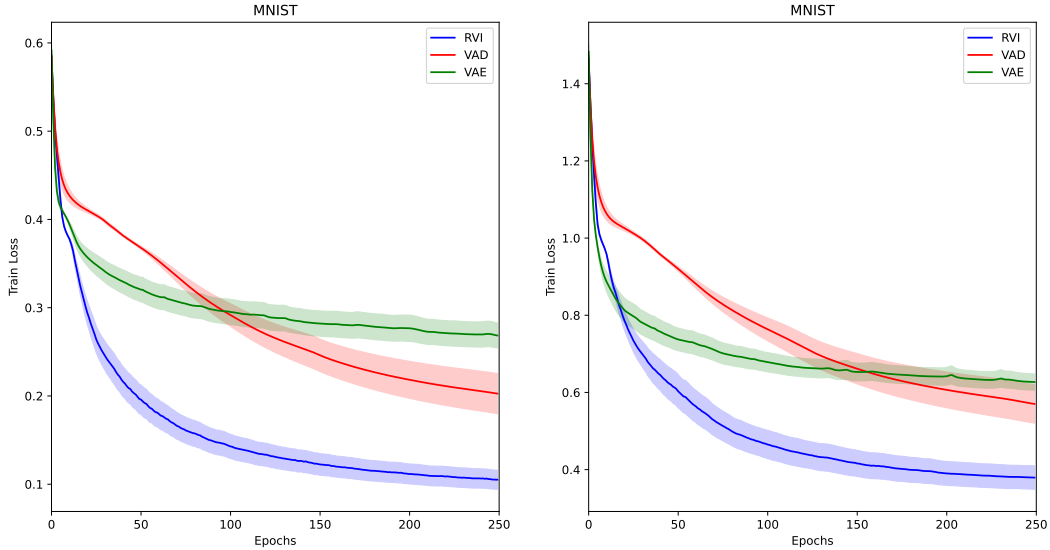


Figure 11: Results for the boxes missing pattern. Right shows the 10 missing, and left 20 missing boxes of 4×4 pixels.

D Further Training Details

The training optimizer for all the experiments is Adam [10]. We set the batch size for the datasets at 256. Due to heavy computational costs associated with the large number of experiments in this paper, we set the maximum data training size at random 10,000 datapoints for the MNIST, FashionMNIST and Artificial datasets. In our experiments 10,000 datapoints were enough to establish comparisons, as the results closely followed the full dataset experiments.

E Choice of Missing Patterns

While in the main body we study the case of MCAR, we also study the case of 10 and 20 missing boxes of 4×4 pixels. Figure 11 shows the results of this experiment, with a similar trend as the MCAR.

F Code

Training code for RVI with all the formulations in Section A are zipped and attached.